Article

Removal of Methyl Violet from Aqueous Solution by Adsorption onto Halloysite Nanoclay: Experiment and Theory

Makfire Sadiku [1], Teuta Selimi [1], Avni Berisha [1], Arsim Maloku [1], Valbonë Mehmeti [2], Veprim Thaçi [1] and Naim Hasani [3,*]

[1] Department of Chemistry, Faculty of Natural and Mathematics Science, University of Prishtina, 10000 Prishtina, Kosovo; makfire.sadiku@uni-pr.edu (M.S.); teutaselimi3@gmail.com (T.S.); avni.berisha@uni-pr.edu (A.B.); arsim.maloku@uni-pr.edu (A.M.); veprim.thaci@uni-pr.edu (V.T.)
[2] Faculty of Agriculture and Veterinary Medicine, University of Prishtina, 10000 Prishtina, Kosovo; valbonamehmeti1@gmail.com
[3] Department of Hydrotechnics, Faculty Civil Engineering, University of Prishtina, 10000 Prishtina, Kosovo
* Correspondence: naim.hasani@uni-pr.edu

Abstract: Methyl Violet (MV) was removed from aqueous solutions by adsorption onto halloysite nanoclay (HNC) employing equilibrium, kinetics, thermodynamic data, molecular modellingR (MD), and Monte Carlo (MC) simulations. The chosen experimental variables were pH, temperature, starting MV concentration, contact time, and adsorbent dosage. The adsorption rate was determined to increase with increasing contact time, initial dye concentration, pH, and temperature. The Langmuir, Freundlich, Temkin, and Dubinin–Radushkevich (D-R) isotherms were utilized to determine the adsorption capacity of HNC. The Langmuir equation matched equilibrium data better than the other models, whereas the pseudo-second-order model better described kinetic data, and thermodynamic analyses revealed that the adsorption process was spontaneous, endothermic, and physisorption-based. This study focused on two distinct molecular mechanics-based theoretical approaches (MC and MD). These techniques enabled a molecular comprehension of the interaction between the MV molecule and the halloysite surface. Theoretical results were consistent with experimental findings. The outcomes revealed that HNC is an excellent dye adsorbent for industrial effluents.

Keywords: halloysite; methyl violet; molecular modelling; monte carlo; adsorption

1. Introduction

Water is a crucial component for life, human evolution, and biodiversity conservation. Unfortunately, human activities have caused a serious degeneration in the quality of water resources. Even though a number of regulations are designed to ensure the safe disposal of industrial effluents, over 80 percent of the world's wastewater is still disposed of without sufficient treatment [1–3]. The release of dye-containing effluents into the natural water bodies can cause harmful effects on the living systems because of their toxic, allergenic, mutagenic, and carcinogenic nature. Dyes obstruct light penetration, impede photosynthetic activity, and as a result, hinder the growth of biota and also cause micro-toxicity to fish and other organisms because of their predisposition to chelate metal ions [4,5].

In several industries such as food, plastic, textile, leather, paper, cosmetics, etc., organic dye effluent is one of the main water pollution problems [6]. Methyl violet (MV) is vital because of its extensive use in textiles, paints, and print inks, and the dying of cotton, silk, paper, and leather, among other applications [7]. MV is also used in medicine as an active ingredient in Gram's biological stain for bacteria categorization [8–11]. Sometimes it can be used as a second-rate disinfectant but has been found to be toxic to most animals. Inhaling MV may irritate the respiratory tract, while ingesting it typically irritates the digestive tract [12,13].

Numerous technologies have been devised and implemented to eliminate synthetic dyes from aqueous solutions and limit their environmental impact [14–18]. Among the methods mentioned above, adsorption is better than the other techniques because of its low cost, simplicity of design, pliability, ease of working, and insensitivity to toxic pollutants [19,20]. Due to this, adsorption is currently recognized as a viable operation for the removal of dyes from the environment; it is a simple and economically viable procedure [21]. Materials such as walnut husk [22], modified chitosan composite [23], biochars from crop residues [24], natural zeolite [25], cross-linked succinyl chitosan [26], modified bentonite [27], quaternized poly(4-vinylpyridine) copolymers [28], natural clinoptilolite [29], activated carbon [30], chromium-intercalated montmorillonite [31], metal oxides [32–35], have been used to remove dyes from aqueous solutions. As well, alumina [36–38], silica gel [39,40], and clay minerals [41–44] are effective and they can support oxidizing environments.

Clay minerals are low-cost, exist in abundance, and are ordinarily innoxious for environmental applications. Their large specific surface area, high porosity, surface charge, and surface functional groups enable the use of clay minerals as adsorbents, flocculants, and filtration media [45,46]. It was discovered that the adsorption capabilities of clays may be greater than those of activated carbon at the same temperature and pH conditions [47]. Adsorption and desorption of organic compounds on clays are primarily determined by the interfacial characteristics of these materials and the chemical properties of their molecules [48]. Clays have a high adsorption capacity for positively charged cations such as cationic dyes, heavy metals, etc., due to their net negative charge.

In this work, the removal of MV from aqueous solutions by adsorption utilizing HNC as an adsorbent was examined. Compared to the earlier published research on the adsorption of MV by HNC published by Liu et al. [49], this work explores the experimental part in more depth and employs theoretical calculations.

The Langmuir, Freundlich, Temkin and Dubinin Radushkeviq (D-R) equations were used to fit the equilibrium isotherms. A kinetic study was carried out with first-order, pseudo first-order, second-order, pseudo second-order, intraparticle and film diffusion models. The thermodynamic parameters derived from adsorption experiments in the present work are extremely useful for elucidating the nature of MV adsorption on halloysite. On the molecular level, the theoretical calculations are of utmost importance as they offer the possibility to evaluate the interaction of molecules on the surfaces. MC and MD provided insights into the theoretical description of the interaction between MV and HNC surface at a molecular level.

2. Materials and Methods

2.1. Adsorbent and Adsorbate

In this study commercial halloysite nanoclay ($Al_2Si_2O_5 (OH)_4 \times 29H_2O$) supplied by Aldrich, was used as an adsorbent.

As adsorbate, Methyl Violet dye purchased from Fluka was utilized and was used without further purification. The stock solution ($1\ g\ L^{-1}$) was prepared by dissolving 1 g of the dye into distilled water. The experimental dye solution was made by diluting the stock solution with the necessary amount of distilled water.

2.2. Batch Experimental Procedure

Batch experiments were performed by stirring 25 mL of known concentration of MV solution with 0.2 g of HNC using magnetic stirrer.

Several parameters such as effect of contact time (1–240 min), effect of initial concentration (100, 125, 150, 175, and 200 mg/L), effect of pH (4–10), and effect of temperature (11, 25, and 40 °C) were done for optimizing the experimental conditions.

The pH was adjusted using 0.1 M HCl and 0.1 M NaOH.

After adsorption, the adsorbent and the supernatants were separated by centrifugation at 5000 rpm for 10 min and samples were investigated for residual dye concentration using a UV–Visible Spectrophotometer (type T70+), at wavelength 579 nm, using a 1 cm quartz cell.

All experiments were repeated three times and mean values were presented with a maximum deviation of 5%.

The amount of MV adsorbed per unit adsorbent (mg/g) was calculated using Equation (1):

$$q_e = \frac{(C_i - C_e) * V}{m} \tag{1}$$

where C_i is the initial dye concentration (mg/L), C_e is the equilibrium dye concentration (mg/L), V is the volume of MV solution used (L), and $m(g)$ is the mass of HNC used.

The MV percent removal was calculated using Equation (2).

$$Removal\ (\%) = \frac{(C_i - C_e) * 100}{C_i} \tag{2}$$

To construct and evaluate an adsorption process, it is necessary to fit equilibrium adsorption data with various adsorption isotherm and kinetic models. Thus, several theoretical models (Table 1) are used for experimental data in order to identify a model that predicts kinetic and isotherm data adequately. The validity of the models was determined by calculating the regression coefficient (R^2) and the root mean square errors (*RMSE*):

$$RMSE = \sqrt{\frac{\Sigma\left(q_{exp} - q_{cal}\right)^2}{N}} \tag{3}$$

where q_{exp} is the experimental value while q_{cal} is the calculated value and N is the number of observations in the experiment. The smaller the *RMSE* values, the better the curve fitting [50,51]. Exel 2016 was used to create all of the graphs.

Table 1. Isotherm, kinetic, and other equations used in this study.

Model	Equation	Parameters
Isotherm models		
Langmuir	$\frac{C_e}{q_e} = \frac{1}{q_m K_L} + \frac{C_e}{q_m}$	q_e (mg g^{-1})—equilibrium adsorption capacity q_m (mg g^{-1})—maximum adsorption capacity K_L (L mg^{-1})—Langmuir constant C_e (mg L^{-1})—equilibrium dye concentration
Freundlich	$\ln q_e = \ln K_F + \frac{1}{n}\ln C_e$	K_F—(mg g^{-1}) (L g^{-1})$^{1/n}$—Freundlich constant n—heterogeneity factor
Temkin	$q_e = \frac{RT}{b_T}\ln K_T + \frac{RT}{b_T}\ln C_e$	K_T (L g^{-1})—Temkin constant related to adsorption capacity. b_T (J mol^{-1})—Temkin constant related to the heat of sorption
Dubinin–Radushkevich (D-R)	$\ln q_e = \ln q_m - \beta\varepsilon^2$ $\varepsilon = RT\ln\left(1 + \frac{1}{C_e}\right)$	β (mol^2/J^2): D-R constant ε (J mol^{-1}): Polanyi potential R (8.314 J mol^{-1} K^{-1})—universal gas constant T (K)—temperature
Kinetic models		
First-order	$\frac{1}{q_t} = \frac{1}{q_e} + \frac{k_1}{q_e t}$	q_t (mg g^{-1}): amount of adsorbate adsorbed at time t k_1 (min^{-1}): first-order rate constant
Pseudo-first-order	$\ln(q_e - q_t) = \ln q_e - k_1 t$	k_1 (min^{-1}): pseudo-first-order rate constant
Second-order	$\frac{1}{C_e} - \frac{1}{C_0} = k_2 t$	k_2 (L mg^{-1} min^{-1}): second-order rate constant
Pseudo-second order	$\frac{t}{q_t} = \frac{1}{k_2 q_e^2} + \frac{t}{q_e}$	k_2 (g mg^{-1} min^{-1}): pseudo-second-order rate constant
Intraparticle-diffusion	$q_t = K_i t^{1/2} + C$	k_i (mg g^{-1} min$^{-0.5}$): intraparticle diffusion rate constant
Liquid film diffusion	$\ln(1 - F) = k_{fd} t + C$ $F = \frac{q_t}{q_e}$	F—fractional attainment of equilibrium, equal to q_t/q_e

2.3. Molecular Modelling and Monte Carlo Calculations

2.3.1. MV and HNC Molecular Modelling

For the interaction amongst the HNC surface and the MV molecule (Figure 1) in the Monte Carlo (MC) and Molecular dynamic (MD) calculations, the simulation was done using the halloysite model (under Periodic Boundary Condition) with cell size of: $61.80 \text{ Å} \times 53.40 \text{ Å} \times 30.14 \text{ Å}$ with the inclusion of a 25 Å vacuum layer at C axis containing inside 2500 water molecules and 1 MV molecule.
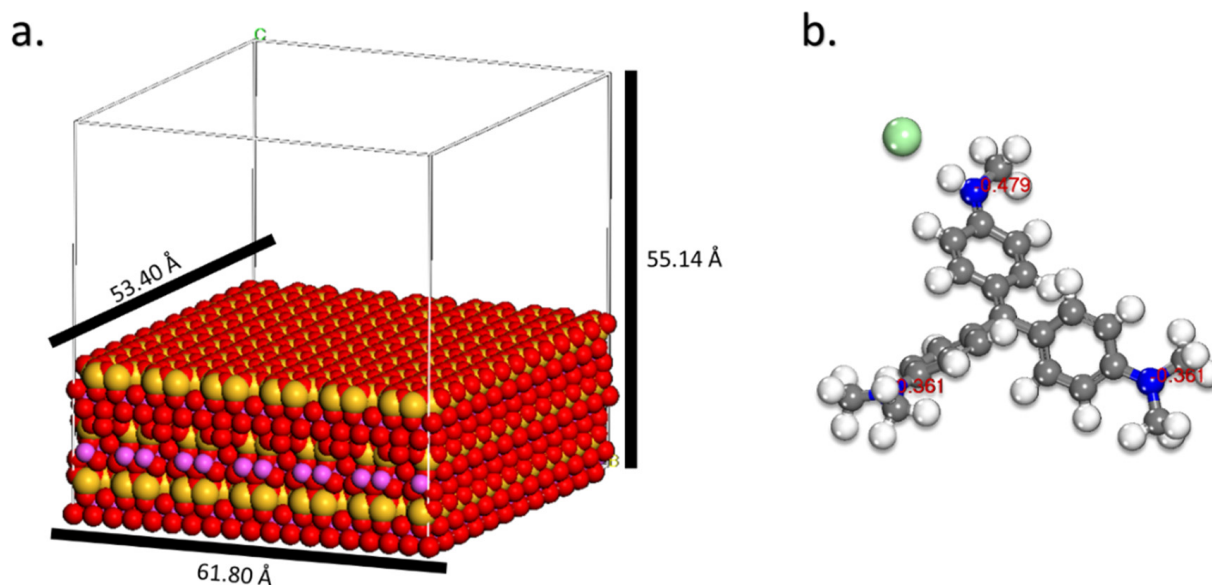

Figure 1. Molecular models used in the theoretical calculations: (**a**) HNC surface, (**b**) MV molecule (with MAC charges).

2.3.2. Monte Carlo and Molecular Dynamic Simulation Details

Six cycles of simulated annealing, each with 15,000 steps, were used to do the MC computations. The annealing temperature was automatically selected between 10^5 and 10^2 K for each cycle. As the temperature steadily decreased, potential adsorption structures were uncovered [52,53]. The MD is performed under an NVT ensemble at 25 °C with a 1 fs time step and 1 ns total simulation period. The temperature control is realized using the Berendsen thermostat MD [54]. MC and MD simulations use COMPASS II's force field. Radial Distribution Function (RDF) is computed using 1 ns of MD trajectory [55,56].

3. Results and Discussion

3.1. Effect of pH

Solution pH affects adsorption. It affects the adsorbent's surface charge, the solution's ionization, and the dissociation of functional groups on the active sites, as well as solution dye chemistry [57,58]. Figure 2 shows the effect of pH on MV removal effectiveness from 4.0 to 10.5. As illustrated in Figure 2, the pH rise from 4 to 10.5, has an insignificant effect on the adsorption capacity. This is in line with other studies such as the adsorption of methyl violet on halloysite nanotube [49] and the adsorption of MG on treated ginger waste [59].

3.2. Effect of Contact Time and Initial Concentration

In Figure 3, the effects of the initial concentrations of MV (100, 125, 150, 175, and 200 mg/L) and contact time (1–240 min) on the adsorption capacity of HNC at 298.15 K are shown.
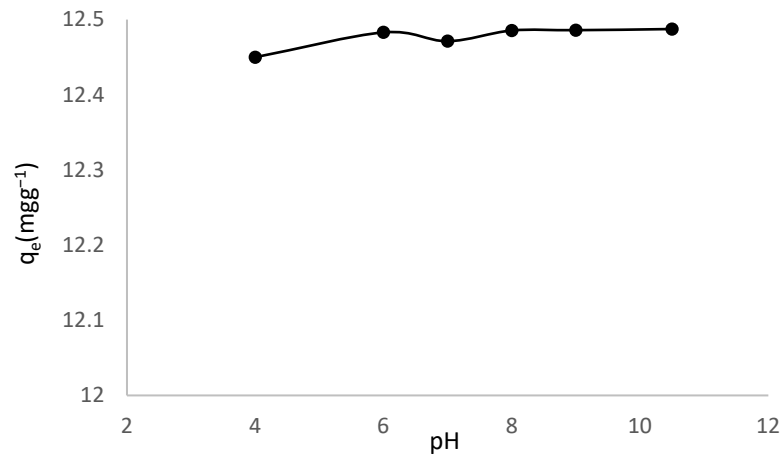
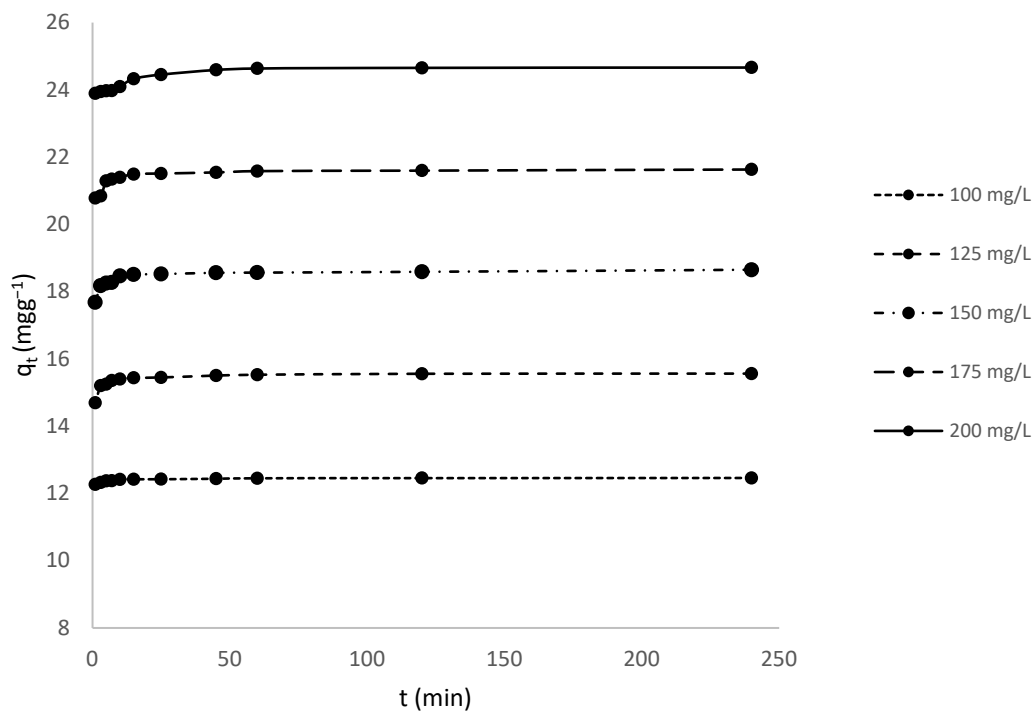**Figure 2.** Effect of pH on adsorption of MV onto HNC.

Figure 3. Time and dye concentration affect MV adsorption on HNC.

MV adsorption was faster in the first 10 min, but slowed when the halloysite became saturated, reaching equilibrium after 240 min. High beginning adsorption rates may be owing to a large number of binding sites, whereas lower rates at the end are due to saturation and equilibrium. Similar conclusions have been proposed [60] for the adsorption of MG by neem sawdust.

Also, adsorption increases with increasing initial dye concentration. According to the results obtained, adsorption capacity increased from 12.46 mg/g to 24.66 mg/g as the initial concentration of MV dye increased from 100 mg/L to 200 mg/L. As initial concentration increases, mass transfer driving force overcomes resistances to dye molecule mass transfer from solution to the solid phase. Also, increasing concentration promotes dye adsorption by increasing dye-halloysite interaction [61,62].

3.3. Effect of Adsorbent Dosage

It was noticed (Figure 4), that the percent of MV adsorption grew significantly from 91–99.9%, with the increase of adsorbent dosage from 0.025 to 0.2 g. Thereafter, by increasing the adsorbent dosage up to 0.4 g, an insignificant increase in the removal efficiency was observed [63].
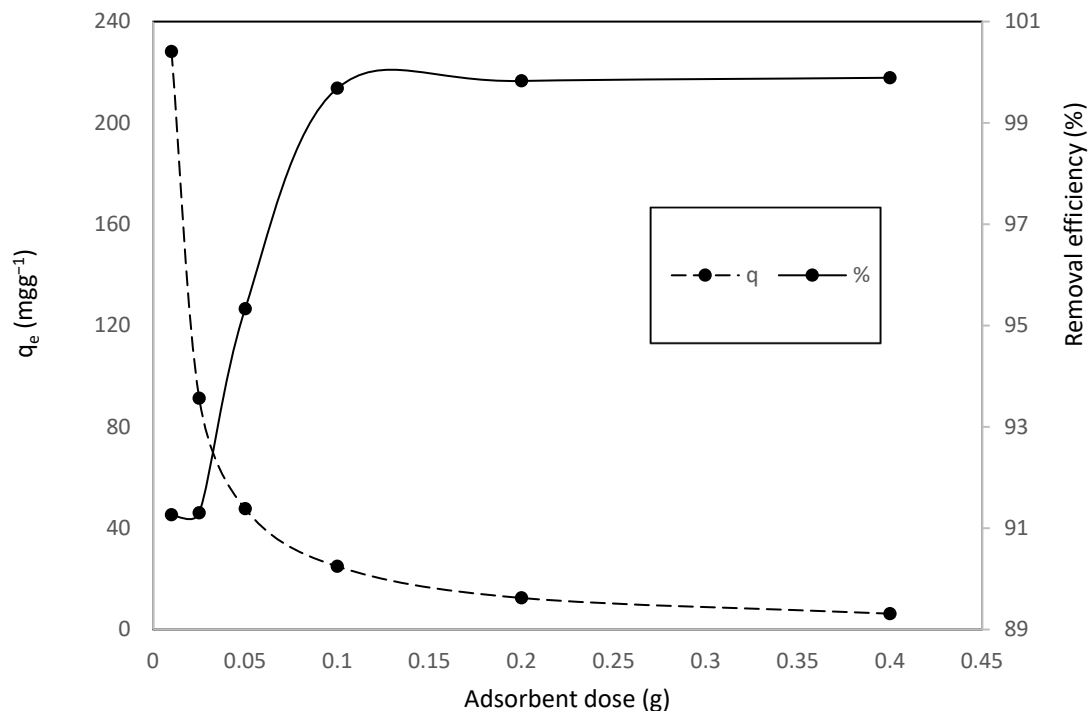

Figure 4. Effect of adsorbent dosage on adsorption of of MV onto HNC.

It was also found that the enhancement of adsorbent dosage, resulted in a decrease in the amount of adsorbed dye per unit mass of adsorbent, from 91.3 to 6.3 mg/g.

Due to a divide in the concentration gradient between dye concentration in the solution and dye concentration on the HNC surface, q_e (mg/g) decreases with increasing adsorbent mass [64].

A similar way of behaving was reported for mercury (II) removal on EB [65] and MB adsorption on guava leaf [66], on gulmohar plant leaf [67], and on cashew nutshell activated carbon [68].

3.4. Effect of Temperature

The effect of temperature on MV dye adsorption onto HNC is introduced in Figure 5.

The equilibrium adsorption capacity of MV onto HNC was found to increase slightly with increasing temperature, from 18.63 mg/g at 284.15 K to 18.71 mg/g at 313.15 K. With increasing temperature, the viscosity of the solution decreases, and consequently the rate of diffusion of dye molecules increases. This leads to an increase in mobility of molecules from the bulk solution to the surface of the adsorbent, and as a result, an increase in the amount of MV adsorbed [69,70].

A similar temperature effect was reported for adsorption of MV adsorption by clinoptilolite [71] and adsorption of the dyestuff astrazon red violet 3 rn (basic violet 16) on montmorillonite clay [72].
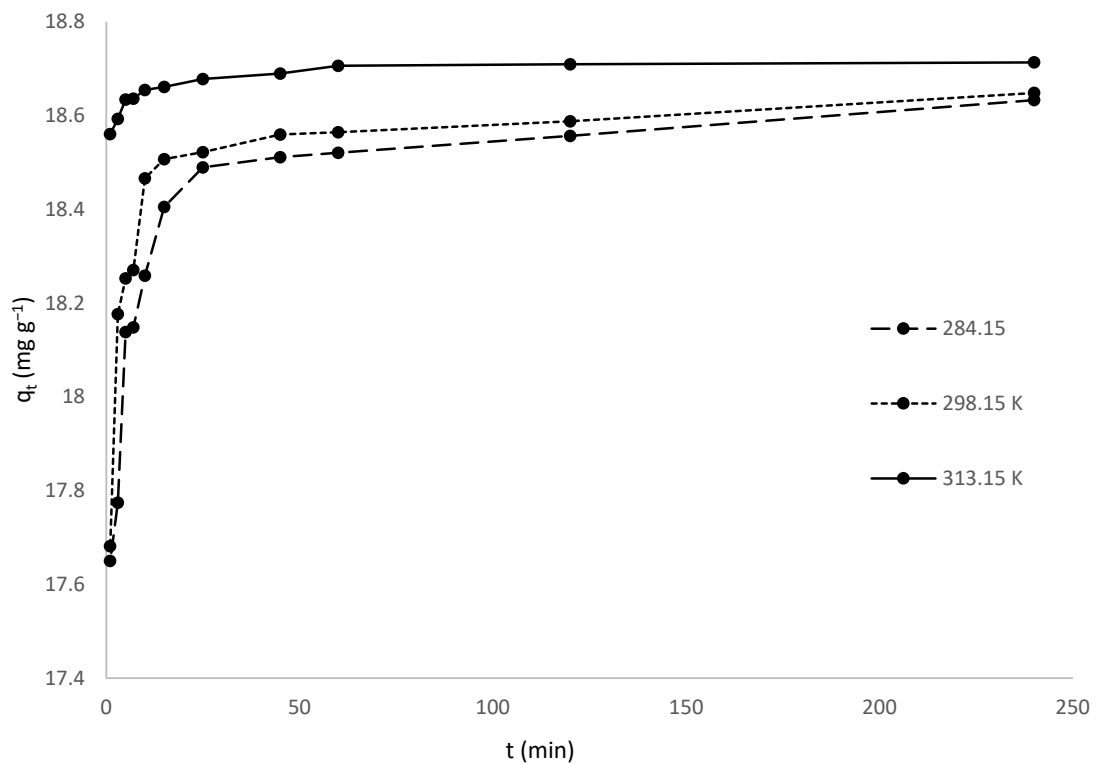
Figure 5. Effect of temperature on adsorption of MV onto HNC.

3.5. Adsorption Isotherms

Four isotherm equations specifically Langmuir, Freundlich, Temkin and Dubinin–Radushkevich (D-R) (Table 1) were employed to interpret the experimental data for MV adsorption on HNC at different temperatures.

The results are shown in Table 2.

Table 2. Isotherm parameters for the adsorption of MV onto HNC.

Model		Parameters			
	Equation		**284.15 K**	**298.15 K**	**313.15 K**
Langmuir	$q_e = \frac{q_m b C_e}{1 + b C_e}$	q_m (mg g^{-1})	27.8550	27.7000	25.3800
		K_L (L mg^{-1})	2.0200	2.3900	8.9500
		R_L	0.0025	0.0021	0.0006
		R^2	0.9990	0.9940	0.9998
		RMSE	0.4700	0.6500	0.7000
Freundlich	$q_e = K_F C_e^{1/n}$	K_F (mg g^{-1})	17.5700	18.4000	21.0800
		n	3.3200	3.3300	5.3600
		R^2	0.9600	0.9575	0.8086
		RMSE	0.9200	0.8000	1.9900
Temkin	$q_e = \frac{RT}{b_T} \ln(K_T C_e)$	K_T (L mg^{-1})	27.9300	32.7200	529.1100
		RT/b (kJ/mol)	5.4310	5.4220	3.4400
		b_T (J mol^{-1})	435.0000	457.1800	755.7800
		R^2	0.9834	0.9770	0.8642
		RMSE	0.5500	0.6400	9.7100
D-R	$q_e = q_m \exp(-\beta \varepsilon^2)$	q_m (mg g^{-1})	23.0100	23.9700	24.8300
		β	7×10^{-8}	6×10^{-8}	2×10^{-8}
		E (kJ/mol)	2.6720	2.890	5.000
		R^2	0.9402	0.9761	0.9811
		RMSE	1.1600	0.8400	6.6000

Based on the R^2, RMSE values, $q_{e,calc}$ values, and modelled isotherms, the Langmuir isotherm model fitted best amongst all the isotherm models investigated. Langmuir

isotherm model assumes similar, energetically equivalent adsorption sites and monolayer adsorption [73].

The Langmuir isotherm constants, K_L and q_m, were calculated from the slope and intercept respectively, of linear plot of C_e/q_e against C_e (Figure 5 and Table 2).

The separation factor (R_L), an essential parameter of the Langmuir isotherm, is generally used to show if the adsorption process is unfavorable ($R_L > 1$), linear ($R_L = 1$), favorable ($0 < R_L > 1$), or irreversible ($R_L = 0$). It can be calculated by Equation (4).

$$R_L = \frac{1}{1 + K_L C_i} \tag{4}$$

The values of R_L in Table 2 indicate that the adsorption of MV on HNC is favorable.

The Freundlich isotherm which assumes multilayer sorption on the heterogeneous adsorbent surface was also utilized to evaluate experimental data. K_F and $1/n$ were calculated from the intercept and slope of the linear plot of log q_e versus log C_e. The values of n greater than unity in Freundlich adsorption isotherm, for all temperatures, indicated that the HNC is suitable for the adsorption of MV.

The Temkin isotherm model includes a factor that takes into account the interactions between the adsorbent and adsorbate. The heat of molecular adsorption in the layer would reduce due to these interactions and the adsorption is identified by a dissipation of binding energies. The determined Temkin parameters (b_T and K_T) exhibited that the interactions between the adsorbent surface and the MV dyes are weak and may be a physical adsorption process. The increased value of b_T with temperature also supports increased adsorption efficiency with increasing temperature [74,75].

Dubinin-Radushkevich (D-R) isotherm model determines whether adsorption is physical or chemical. The values of constants q_m and β are given in Table 2. The parameter β could be used to calculate the mean free energy (E = $1/\sqrt{2\beta}$), which could distinguish the type of the adsorption process. If the value of E is less than 8 kJ mol^{-1}, the adsorption process is physical, and when E is between 8 kJ mol^{-1} and 16 kJ mol^{-1}, the process is chemical adsorption [76].

The value of apparent energy E (less than 8.0 kJ mol^{-1}) indicated that the adsorption of MV onto the HNC is a physical process and is consonant with the ΔG parameter results [77].

The nonlinear relationship of the isotherm models used, is shown in Figure 6.
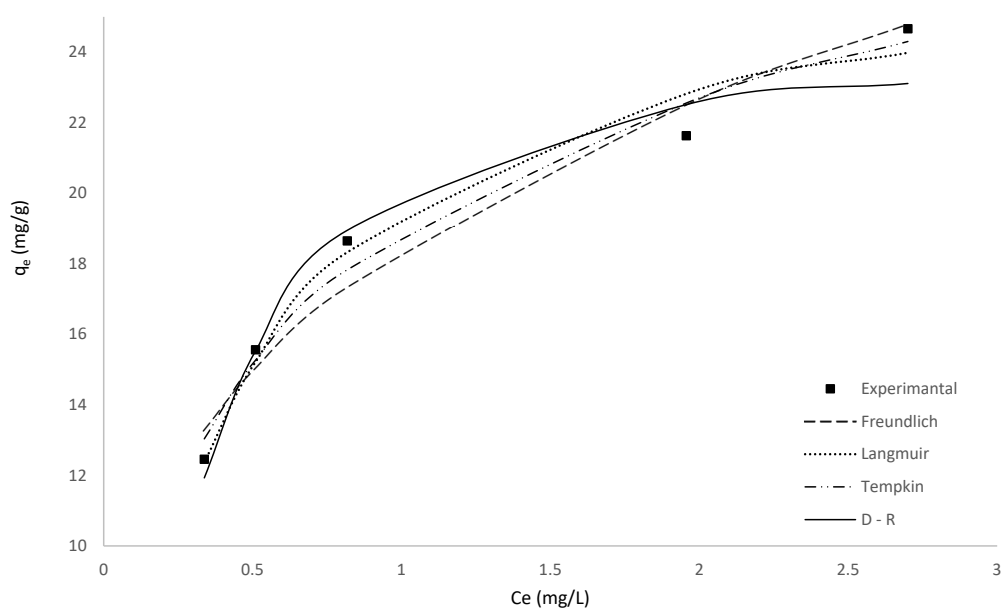

Figure 6. Comparison of the experimental and modelled isotherms for the adsorption of MV by HNC.

3.6. Adsorption Kinetics

In order to investigate the adsorption process and potential rate controlling step of MV adsorption onto HNC first order, pseudo-first-order, second order, pseudo-second-order, and intra-particle diffusion kinetic models were studied (Table 1).

Figure 7 shows the linear relationship of kinetic models for the MV adsorption process and the value of kinetics parameters determined using these models are given in Table 3.
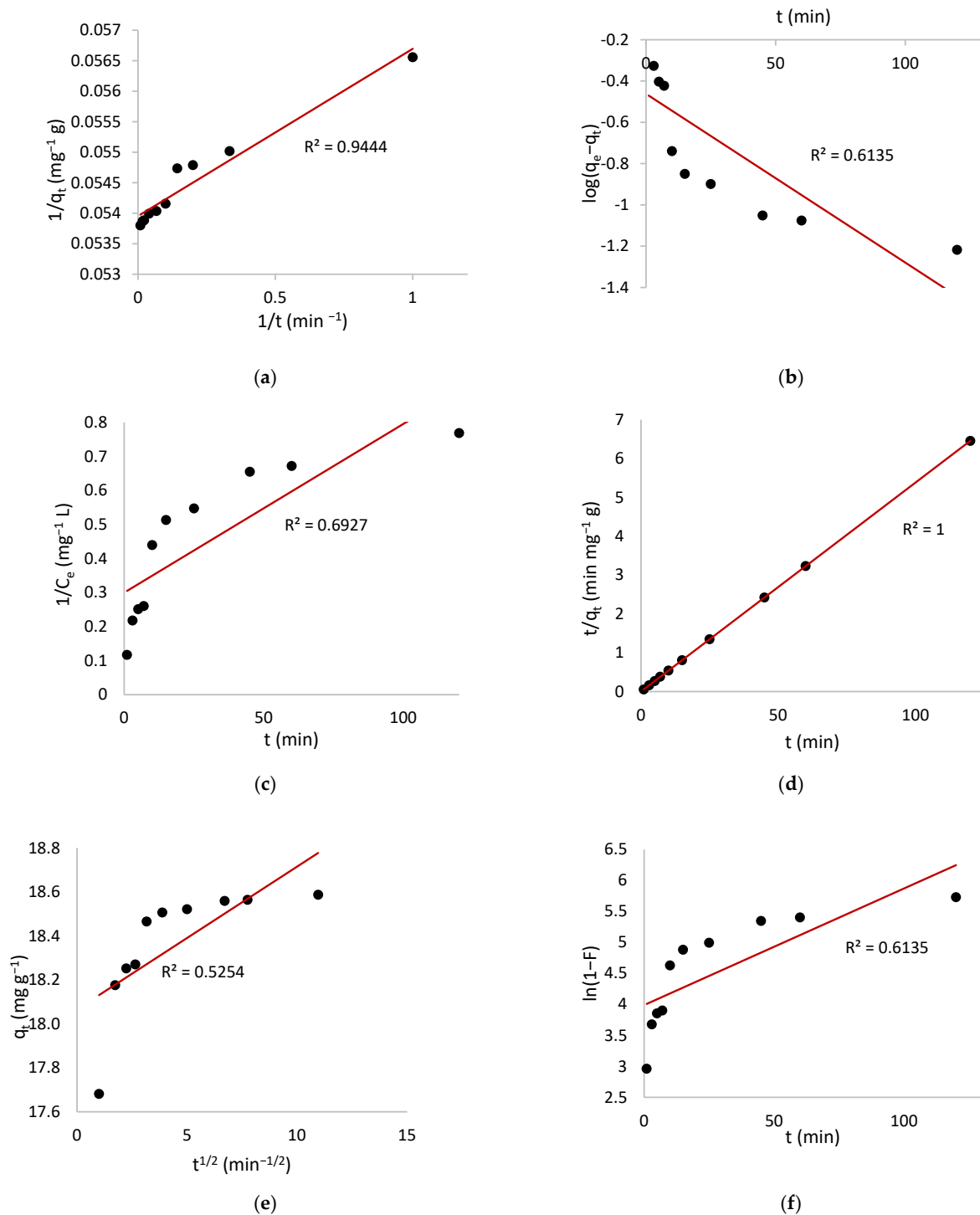

Figure 7. Kinetic model plots for MV adsorption onto HNC (**a**) first order, (**b**) pseudo-first order, (**c**) (second order, (**d**) pseudo-second order, (**e**) intraparticle diffusion and (**f**) liquid film diffusion.

Table 3. Comparison of HNC adsorption capacities with various adsorbents.

Adsorbent	q_{max}/mg g^{-1}	Ref
Natural and Zwitterionic Surfactant-modified Clay	54.61	[1]
Halloysite Nanotubes	187.18	[46]
DTMA-bentonite	740.5	[48]
Lignit coal	40.82	[50]
Halloysite Nanotubes	97.96	[75]
Halloysite Nanotubes	84.32	[78]
Na-bentonite	67.1	[48]
Magnetic composite	20.04	[13]
HNC	27.7	This study

On the basis of the high values of the regression coefficient, (R = 1) and very close values of $q_{e,calc}$ with $q_{e,exp}$, the pseudo-second-order rate model fitted the experimental data better than any other model studied, providing evidence that the adsorption of MV on HNC followed the pseudo-second-order kinetic model. Considerable reduction of dye amount during batch adsorption experiments and longer time needed for adsorbing species to diffuse to remote locations deep within a network of fine pores are the two contributing explanations for these results [79,80].

Similar findings are also reported for adsorption of methylene blue by coconut husks/polylactide blended films [81], adsorption of CV dye on zeolites from coal fly and bottom ashes [78], and adsorption of CV dye on coffee husks [82].

Adsorbate molecules travel from the aqueous phase to the adsorbent surface, then diffuse into pores. External mass transfer (boundary layer diffusion) or intraparticle diffusion determines the adsorption rate. The experimental adsorption kinetics data were fitted using the intraparticle diffusion model and the liquid film diffusion model to determine the rate-determining step.

If the intraparticle diffusion is the sole rate-limiting step, the plot of q_t vs. $t^{0.5}$ gives a straight line with zero intercept. As the intraparticle diffusion plot did not pass through the origin some other mechanism might be included. For that reason, the kinetic data were examined by the liquid film diffusion model. Linear graphs of ln (1 − F) vs. t with zero intercept suggest that adsorption kinetics are driven by diffusion through the liquid film surrounding solid adsorbents. The low values of R^2 (Table 4) and the non-zero intercept plots of the liquid film diffusion model indicate that the liquid film diffusion is also not the sole rate-determining step.

Table 4. Kinetic parameters for the sorption of MV onto HNC.

Model	$q_{e,exp}$ (mg g^{-1})	Parameters	
First-order		k_1 (min^{-1})	0.0500
		$q_{e,calc}$ (mg g^{-1})	18.5200
		R^2	0.9444
Pseudo first-order		k_1 (min^{-1})	0.0188
		$q_{e,calc}$ (mg g^{-1})	0.3450
		R^2	0.6135
Second-order		k_2 (g mg^{-1} min^{-1})	0.0050
	18.648	R^2	0.6927
Pseudo second-order		k_2 (gmg^{-1} min^{-1})	0.6300
		$q_{e,calc}$ (mg g^{-1})	18.5900
		R^2	1
Intrapaticle diffusion		k_i (mg g^{-1} min$^{-1/2}$)	0.0650
		C	18.0700
		R^2	0.5254
Liquid film diffusion		K_{fd}	0.0188
		C	3.9895
		R^2	0.6135

So the adsorption mechanism is a combination of the two processes mentioned above [51,77].

3.7. Adsorption Thermodynamics

The free energy change (ΔG^0), enthalpy change (ΔH^0), and entropy change (ΔS^0) were evaluated using the following equations:

$$\Delta G^0 = -RT \, lnK_c \tag{5}$$

$$lnK_c = \frac{\Delta S^0}{R} - \frac{\Delta H^0}{RT} \tag{6}$$

$$K_c = K_L \times 10^6 \tag{7}$$

where Kc is the equilibrium constant (dimensionless), [83,84] R is the gas constant (J/Kmol), and T is the temperature (K).

The ΔH^0 and ΔS^0 were determined from the slope and intercept of the plot of lnK_c versus 1/T (Figure 8), and the results are shown in Table 5.
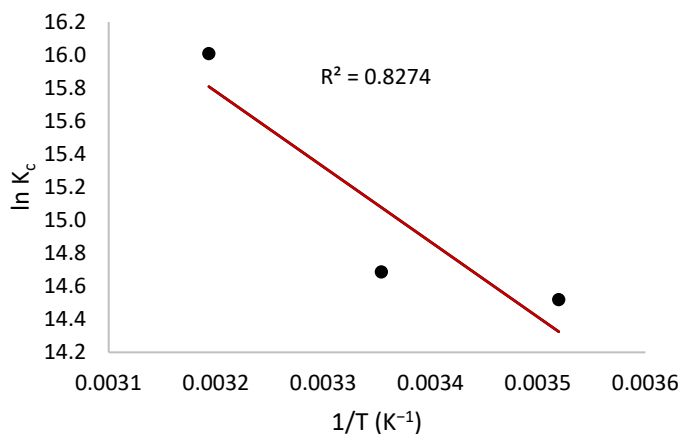

Figure 8. Plot of ln Kc versus $1/T$ of the adsorption process.

Table 5. The thermodynamic parameters of adsorption of MV onto HNC.

Temperature (K)	ΔG^0 (kJ/mol)	ΔH^0 (kJ/mol)	ΔS^0 (J/mol K)
313.15	−41.68		
298.15	−36.40	37.84	252.30
284.15	−34.30		

The positive value of ΔH^0 (+37.84 kJ/mol) indicated that the adsorption process was endothermic and since this value is less than 80 kJ/mol (80 kJ/mol is the upper limit of the change of enthalpy for physisorption), it shows that the adsorption follows a physisorption.

The positive value of ΔS^0 indicated increased disorder and randomness at the solid-liquid interface; however, the negative value of ΔG^0 suggested spontaneous and thermodynamically favorable adsorption of MV onto HNC.

Meantime, the value of ΔG^0 became more negative with increasing temperature, which exhibits that higher temperature is contributory to adsorption [19].

The activation energy Ea was obtained using the Arrhenius equation:

$$lnk_2 = lnA - \frac{E_a}{RT} \tag{8}$$

where k_2 is the pseudo-second-order rate constant, A is the Arrhenius constant, E_a refers to the energy of activation (J mol^{-1}), R is the ideal gas constant (8.314 J mol^{-1} K^{-1}), and T is the temperature (K).

The slope of the plot of *ln* k_2 versus $1/T$ (Figure 9) is used to evaluate E_a, which was found to be 44 kJ/mol.
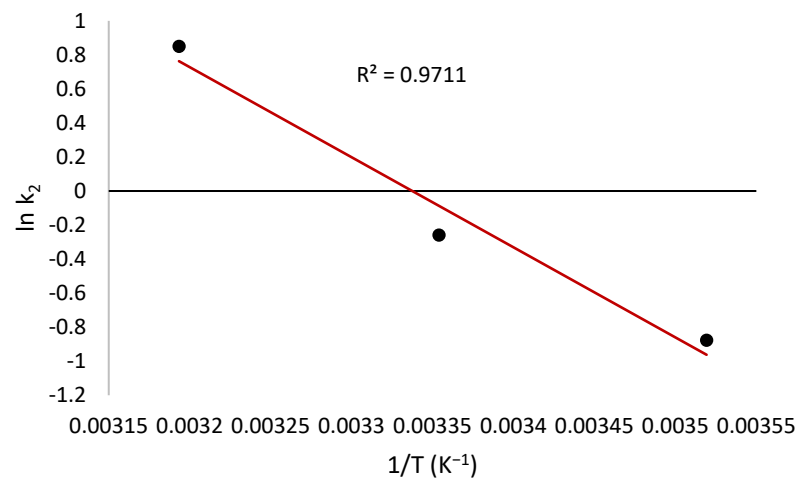

Figure 9. Plot of ln k_2 versus $1/T$ of the adsorption process.

This value is consistent with the values of the activation energy (43.0 kJ/mol) for the adsorption of reactive red 189 on cross-linked chitosan beads [85], and (5.6–49.1 kJ/mol) for the adsorption of polychlorinated biphenyls on fly ash [86].

3.8. Monte Carlo and Molecular Dynamic Simulations

Figure 10 depicts the lowest energy configurations for the MV on the HNC surface under the simulated adsorption circumstances that were employed (as chosen above). As evidenced by Mulliken charges (Figure 1), the adsorption geometries of the MV demonstrate that nitrogen atoms are mostly responsible for this behavior.
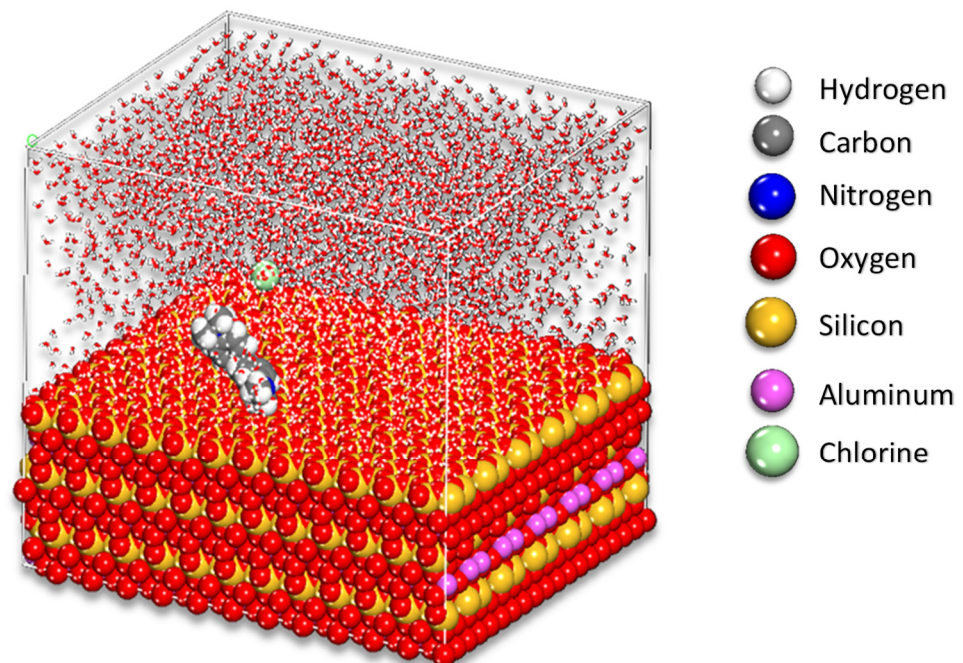

Figure 10. Final MC poses of the lowest adsorption configurations for the MV in the simulated corrosion media on the HNC surface PBC model.

The following equation may be used to calculate the adsorption energies of the adsorbate molecule on the halloysite surface.

$$E_{ads} = E_{total} - \left[E_{surface+water} + E_{MV+surface} \right] + E_{water} \qquad (9)$$

where: E_{total} is the total energy of the system as a result of adsorbent-adsorbate; $E_{surface+water}$ and $E_{MV+water}$ is system energy in the absence and presence of MV.

Figure 11 depicts the distribution of the adsorption energies for the large number of adsorptive configurations developed and computed by the Monte Carlo approach for the MV adsorbate, which was based on the results of the Monte Carlo method.
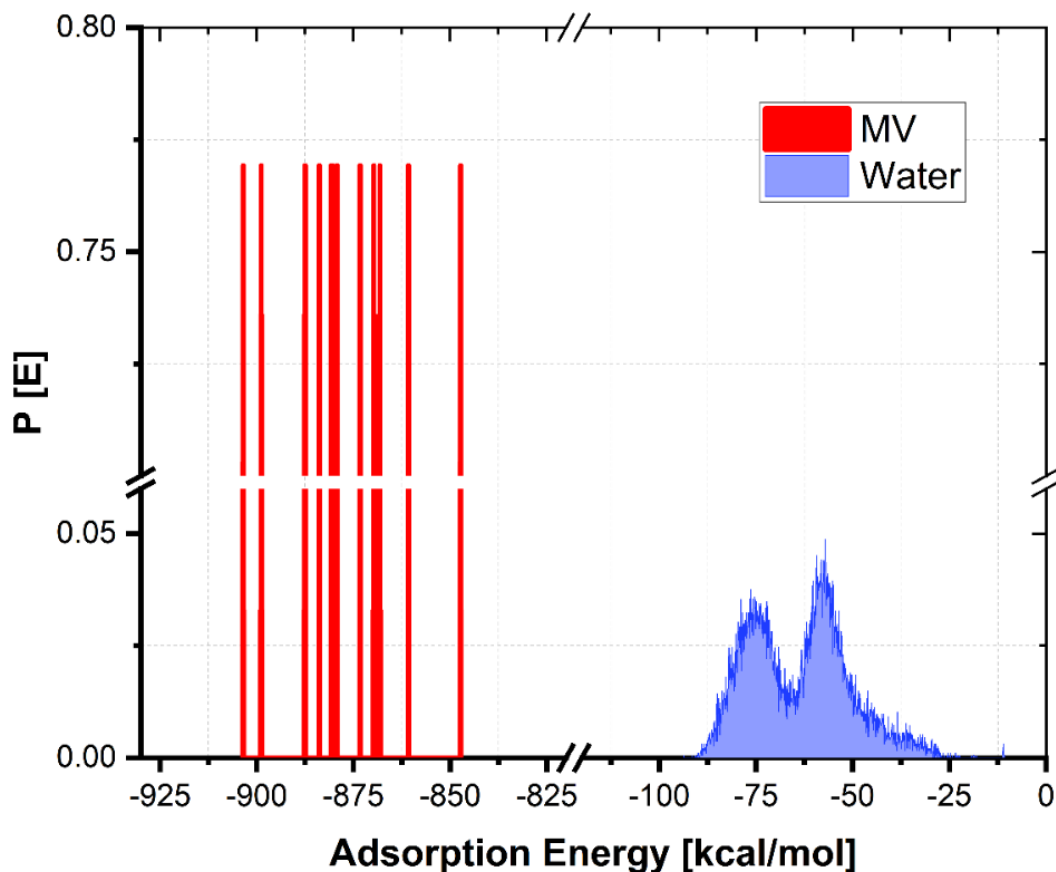

Figure 11. Distribution of adsorption energies for MV onto the halloysite surface.

The Adsorption Energy (E_{ads}) values for the adsorption of MV onto the HNC surface are presented in Table 6.

Table 6. The distribution E_{ads} values for MV onto the Halloysite surface.

Molecule	Adsorption Media		
	Min.	Max.	Mean Value
MV	−847.15	−903.55	−875.35

As indicated by the high E_{ads}, the MV has a strong contact with the halloysite surface, resulting in good adsorptive properties. Adsorption of MV onto the halloysite surface was determined by both the MC and MD calculations, respectively. In the case of the adsorption process, Monte Carlo simulations (see Figures 10 and 12) have indicated that the ensuing negative values of adsorption are indicative of the spontaneity with which the process occurs (Figure 11). It is important to employ MD simulations because they give

a very simple means of tracking and recording the kinetics of inhibitor adsorption on the metal surface under study. Figure 12 shows the final arrangements of MV on the halloysite surface as depicted in the previous figure.
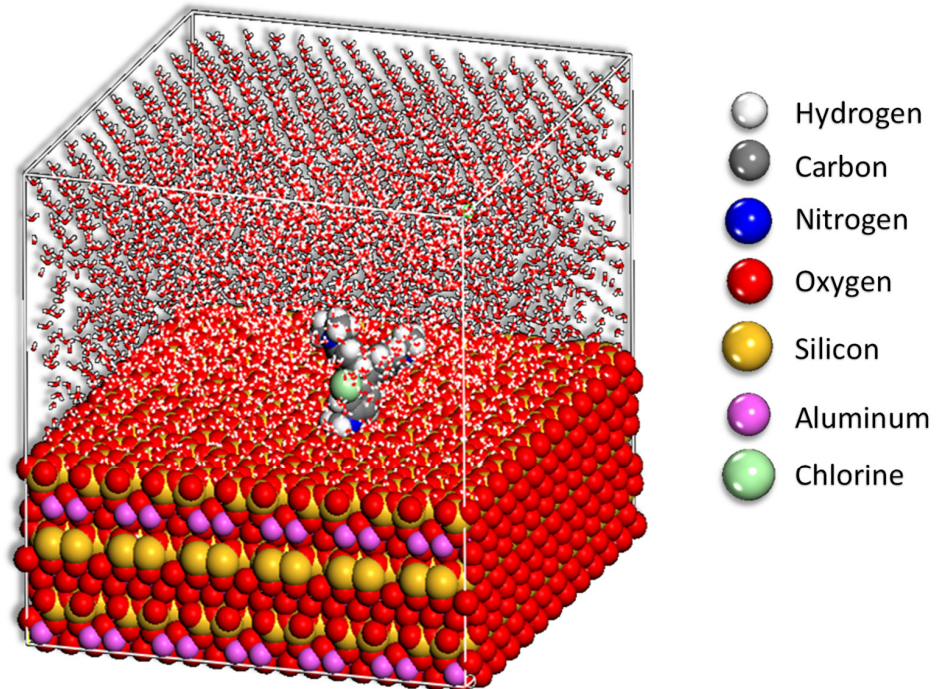

Figure 12. Final MD pose of the lowest adsorption configurations for the MV in the simulated corrosion media on the HNC surface PBC model.

The presence of an RDF peak between 1 and 3.5 Å from the surface plane of the material and the adsorbate atom confirms adsorption, but for physisorption, RDF peaks at greater distances confirm physisorption, and vice versa.

The RDF of the nitrogen atoms in the MV (Figure 13 is close to the surface plane, suggesting that these components have an increased interaction with the adsorbent surface. The findings of the MD and RDF analyses confirm that these inhibitors have a high proclivity to adsorb onto the surface, owing to their peculiar attraction to share and accept electrons with the surface in question. [55].
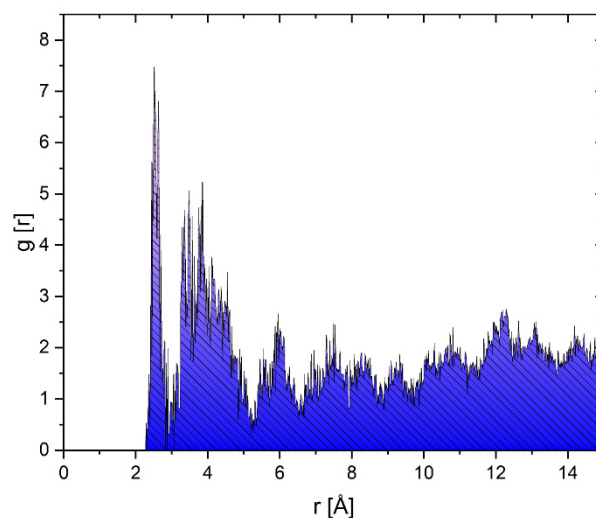

Figure 13. RDF of nitrogen MV the halloysite surface obtained via MD.

3.9. FTIR Spectroscopy

FTIR-8400S was used for Total Attenuated Reflection (ATR) measurements with the following parameters: resolution 2 cm^{-1}, 100 scans, 500–4000 cm^{-1}. Figure 14 exhibits the peaks that appeared at certain wave numbers of MV FTIR spectra before and after adsorption onto HNC.

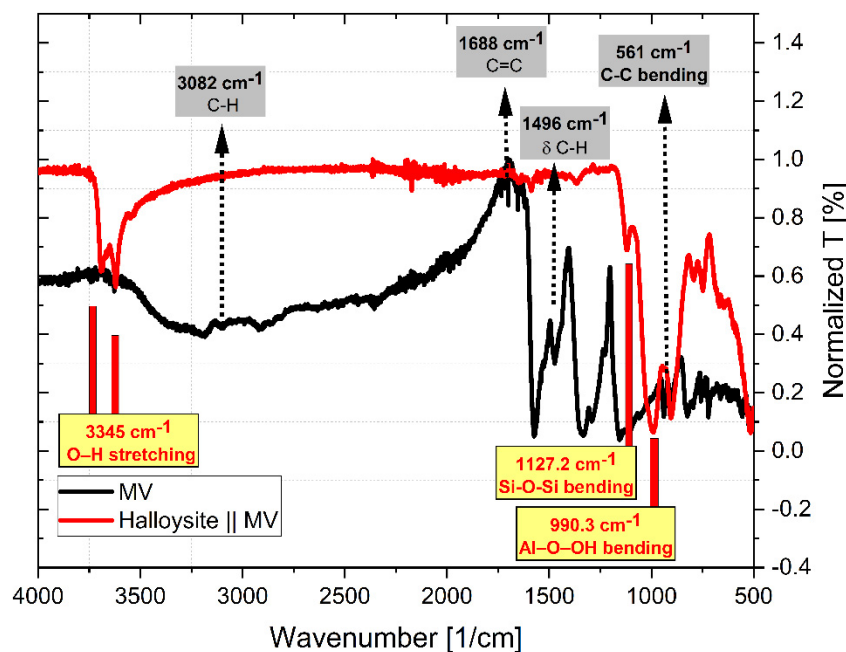**Figure 14.** The FTIR spectrum of MV and MV-HNC.

The following peaks: 3082 and 1496 cm^{-1} show -CH- aromatic and 2927 cm^{-1} –CH$_3$ methyl vibrating vibrations, respectively 1688 cm^{-1}, aromatic ring vibrations –C=C– vibrations from the skeleton of aromatic ring structures of MV, while we have new displays of vibrations of the group -OH at 3345 cm^{-1} stretching, 1127.2 cm^{-1} bending by the group connections -Si-O-Si- bending and 990.3 cm^{-1} from the -Al-O-OH- bond arising from the Halloysite and MV groups with distinctive features (as shown in Figure 14).

The interaction of MV molecules with Halloysite functional groups was confirmed by the emergence and disappearance or depletion of various peaks.

4. Conclusions

This study established the viability of halloysite nanoclay as a dye-removal adsorbent in wastewater. The findings of the batch trials revealed that adsorption was affected by adsorbent dose, contact time, initial dye concentration, and temperature.

Adsorption of MV is very little affected by changing the temperature and pH. The optimal adsorption capacity (27.7 mg/g) was reached at ambient temperature (298 K) and pH (4.26).

Among the investigated isotherm models, the Langmuir isotherm model demonstrated the best fit.

The experimental data were best suited by the pseudo-second-order rate model, indicating that the adsorption of MV on HNC followed the pseudo-second-order kinetic model. The kinetic analysis indicated that the adsorption mechanism is a combination of intra-particle diffusion and film diffusion.

Thermodynamic investigations demonstrated that the removal of MV by HNC is possible, exothermic, and spontaneous.

This study focuses on two distinct molecular mechanics-based theoretical approaches (MC and MD). These techniques enabled a molecular comprehension of the interaction between the MV molecule and the halloysite surface. Simulations using Monte Carlo and

molecular dynamics revealed that this molecule spontaneously adsorbs onto surfaces. The negative value of the adsorption energies supports a strong interaction between the MV and HNC surface, which is consistent with experimental findings.

References

1. Abdel Ghafar, H.H.; Radwan, K.E.; El-Wakeel, T.S. Removal of Hazardous Contaminants from Water by Natural and Zwitterionic Surfactant-modified Clay. *ACS Omega* **2020**, *5*, 6834–6845. [CrossRef] [PubMed]
2. Da Silva, B.C.; Zanutto, A.; Pietrobelli, J.M. Biosorption of reactive yellow dye by malt bagasse. *Adsorpt. Sci. Technol.* **2019**, *37*, 236–259. [CrossRef]
3. Conradi, E.; Goncalves, A.C.; Schwantes, D.; Manfrin, J.; Schiller, A.; Zimmerman, J.; Klassen, G.J.; Ziemer, G.L. Development of renewable adsorbent from cigarettes for lead removal from water. *J. Environ. Chem. Eng.* **2019**, *7*, 103200. [CrossRef]
4. Akar, S.T.; Özcan, A.S.; Akar, T.; Özcan, A.; Kaynak, Z. Biosorption of a reactive textile dye from aqueous solutions utilizing an agro-waste. *Desalination* **2009**, *249*, 757–761. [CrossRef]
5. Malik, R.; Ramteke, D.S.; Wate, S.R. Adsorption of malachite green on groundnut shell waste based powdered activated carbon. *Waste Manag.* **2007**, *27*, 1129–1138. [CrossRef] [PubMed]
6. Monvisade, P.; Siriphannon, P. Chitosan intercalated montmorillonite: Preparation, characterization and cationic dye adsorption. *Appl. Clay Sci.* **2009**, *42*, 427–431. [CrossRef]
7. Ofomaja, A.E.; Ukpebor, E.E.; Uzoekwe, S.A. Biosorption of Methyl violet onto palm kernel fiber: Diffusion studies and multistage process design to minimize biosorbent mass and contact time. *Biomass Bioenergy* **2011**, *35*, 4112–4123. [CrossRef]
8. Esteva, M.; Ruiz, A.M.; Stoka, A.M. Trypanosoma cruzi: Methoprene is a potent agent to sterilize blood infected with trypomastigotes. *Exp. Parasitol.* **2002**, *100*, 248–251. [CrossRef]
9. Laube, S. Skin infections and ageing. *Ageing Res. Rev.* **2004**, *3*, 69–89. [CrossRef]
10. Saji, M.; Taguchi, S.; Uchiyama, K.; Osono, E.; Hayama, N.; Ohkuni, H. Efficacy of gentian violet in the eradication of methicillin-resistant Staphylococcus aureus from skin lesions. *J. Hosp. Infect.* **1995**, *31*, 225–228. [CrossRef]
11. Wainwright, M. Dyes for the medical industry. In *Handbook of Textile and Industrial Dyeing*; Woodhead Publishing: London, UK, 2011; pp. 204–230.
12. Li, P.; Su, Y.J.; Wang, Y.; Liu, B.; Sun, L.M. Bioadsorption of methyl violet from aqueous solution onto Pu-erh tea powder. *J. Hazard. Mater.* **2010**, *179*, 43–48. [CrossRef]
13. Bonetto, L.R.; Ferrarini, F.; De Marco, C.; Crespo, J.S.; Guégan, R.; Giovanela, M. Removal of methyl violet 2B dye from aqueous solution using a magnetic composite as an adsorbent. *J. Water Process Eng.* **2015**, *6*, 11–20. [CrossRef]
14. Wu, J.; Eiteman, M.A.; Law, S.E. Evaluation of membrane filtration and ozonation processes for treatment of reactive-dye wastewater. *J. Environ. Eng.* **1998**, *124*, 272–277. [CrossRef]
15. Vimonses, V.; Lei, S.; Jin, B.; Chow, C.W.K.; Saint, C. Kinetic study and equilibrium isotherm analysis of Congo Red adsorption by clay materials. *Chem. Eng. J.* **2009**, *148*, 354–364. [CrossRef]
16. Moghaddam, S.S.; Moghaddam, M.R.A.; Arami, M. Coagulation/flocculation process for dye removal using sludge from water treatment plant: Optimization through response surface methodology. *J. Hazard. Mater.* **2010**, *175*, 651–657. [CrossRef]
17. Hisaindee, S.; Meetani, M.A.; Rauf, M.A. Application of LC-MS to the analysis of advanced oxidation process (AOP) degradation of dye products and reaction mechanisms. *TrAC Trends Anal. Chem.* **2013**, *49*, 31–44. [CrossRef]
18. Turhan, K.; Durukan, I.; Ozturkcan, S.A.; Turgut, Z. Decolorization of textile basic dye in aqueous solution byozone. *Dye. Pigment.* **2012**, *92*, 897–901. [CrossRef]
19. Tong, Z.; Zheng, P.; Bai, B.; Wang, H.; Suo, Y. Adsorption Performance of Methyl Violet via α-Fe$_2$O$_3$@Porous Hollow Carbonaceous Microspheres and Its Effective Regeneration through a Fenton-Like Reaction. *Catalysts* **2016**, *6*, 58. [CrossRef]

20. Wang, L.; Zhang, J.; Zhao, R.; Li, C.; Li, Y.; Zhang, C. Adsorption of basic dyes on activated carbon prepared from Polygonum orientale Linn: Equilibrium, kinetic and thermodynamic studies. *Desalination* **2010**, *254*, 68–74. [CrossRef]

21. Baouch, Z.; Benabadji, K.I.; Bouras, B. Adsorption of Different Dyes from Aqueous Solutions Using Organo-clay Compposites. *Phys. Chem. Res.* **2020**, *8*, 767–787.

22. Çelekli, A.; Birecikligil, S.S.; Geyik, F.; Bozkurt, H. Prediction of removal efficiency of lanaset red G on walnut husk using artificial neural network model. *Bioresour. Technol.* **2012**, *103*, 64–70. [CrossRef]

23. Zhu, H.Y.; Jiang, R.; Fu, Y.Q.; Jiang, J.H.; Xiao, L.; Zeng, G.M. Preparation, characterization and dye adsorption properties of γ-Fe$_2$O$_3$/SiO$_2$/Chitosan Composite. *Appl. Surf. Sci.* **2011**, *258*, 1337–1344. [CrossRef]

24. Xu, R.K.; Xiao, S.C.; Yuan, J.H.; Zhao, A.Z. Adsorption of methyl violet from aqueous solutions by the biochars derived from crop residues. *Bioresour. Technol.* **2011**, *102*, 10293–10298. [CrossRef] [PubMed]

25. Akgül, M.; Karabakan, A. Promoted dye adsorption performance over desilicated natural zeolite. *Microporous Mesoporous Mater.* **2011**, *145*, 157–164. [CrossRef]

26. Huang, X.Y.; Bu, H.T.; Jiang, G.B.; Zeng, M.H. Cross-linked succinyl chitosan as an adsorbent for the removal of methylene blue from aqueous solution. *Int. J. Biol. Macromol.* **2011**, *49*, 643–651. [CrossRef] [PubMed]

27. Heddi, D.; Benkhaled, A.; Boussaid, A.; ChoukchouBraham, E. Adsorption of anionic dyes on poly(N-vinylpyrrolidone) modified bentonite. *Phys. Chem. Res.* **2019**, *7*, 731–749.

28. Medjahed, K.; Tennouga, L.; Mansri, A.; Hammouti, B.; Desbrières, J. Interaction between poly(4-vinylpyridine-graft-bromodecane) and textile blue basic dye by spectrophotometric study. *Res. Chem. Intermed.* **2013**, *39*, 3199–3208. [CrossRef]

29. Ghaedi, M.; Hossainian, H.; Montazerozohori, M.; Shokrollahi, A.; Shojaipour, F.; Soylak, M.; Purkait, M.K. A Novel Acorn Based Adsorbent for the Removal of Brilliant Green. *Desalination* **2011**, *281*, 226–233. [CrossRef]

30. Elmoubarki, R.; Mahjoubi, F.Z.; Tounsadi, H.; Moustadraf, J.; Abdennouri, M.; Zouhri, A.; El Albani, A.; Barka, N. Adsorption of textile dyes on raw and decanted moroccan clays: Kinetics, equilibrium and thermodynamics. *Water Resour. Ind.* **2015**, *9*, 16–29. [CrossRef]

31. Bouberka, Z.; Khenifi, A.; Benderdouche, N.; Derriche, Z. Removal of supranol yellow 4GL by adsorption onto Cr-intercalated montmorillonite. *J. Hazard. Mater.* **2006**, *133*, 154–161. [CrossRef] [PubMed]

32. Mousavi, S.M.; Babapoor, A.; Hashemi, S.A.; Medi, B.C. Adsorption and removal characterization of nitrobenzene by graphene oxide coated by polythiophene nanoparticles. *Phys. Chem. Res.* **2020**, *8*, 225–240.

33. Ait Himi, M.; El Ghachtouli, S.; Amarray, A.; Zaroual, Z.; Bonnaillie, P.; Azzi, M. Removal of azo dye calcon using polyaniline films electrodeposited on SnO$_2$ substrate. *Phys. Chem. Res.* **2020**, *8*, 111–124.

34. Salari, H.; Kohantorabi, M. Fabrication of novel Fe$_2$O$_3$/MoO$_3$/AgBr nanocomposites with enhanced photocatalytic activity under visible light irradiation for organic pollutant degradation. *Adv. Powder Technol.* **2020**, *31*, 493–503. [CrossRef]

35. Salari, H.; Kohantorabi, M. Facile template-free synthesis of new α-MnO$_2$ nanorod/silver iodide p-n junction nanocomposites with high photocatalytic performance. *N. J. Chem.* **2020**, *44*, 7401–7411. [CrossRef]

36. Yahyaei, B.; Azizian, S. Rapid adsorption of binary dye pollutants onto the nanostructred mesoporous alumina. *J. Mol. Liq.* **2014**, *199*, 88–95. [CrossRef]

37. Zolgharnein, J.; Bagtash, M.; Shariatmanesh, T. Simultaneous removal of binary mixture of Brilliant Green and Crystal Violet using derivative spectrophotometric determination, multivariate optimization and adsorption characterization of dyes on surfactant modified nano-γ-alumina. *Spectrochim. Acta Part A Mol. Biomol. Spectrosc.* **2015**, *137*, 1016–1028. [CrossRef] [PubMed]

38. Javadian, H.; Angaji, M.T.; Naushad, M. Synthesis and characterization of polyaniline/γ-alumina nanocomposite: A comparative study for the adsorption of three different anionic dyes. *J. Ind. Eng. Chem.* **2014**, *20*, 3890–3900. [CrossRef]

39. Liu, G.; Yang, R.L. Liquid adsorption of basic dye using silica aerogels with different textural properties. *J. Non-Cryst. Solids* **2010**, *356*, 250–257. [CrossRef]

40. Krysztafkiewicz, A.; Binkowski, S.; Jesionowski, T. Adsorption of dyes on a silica surface. *Appl. Surf. Sci.* **2002**, *199*, 31–39. [CrossRef]

41. Errais, E.; Duplay, J.; Elhabiri, M.; Khodja, M.; Ocampo, R.; Baltenweck-Guyot, R.; Darragi, F. Anionic RR120 dye adsorption onto raw clay: Surface properties and adsorption mechanism. *Colloids Surf. Physicochem. Eng. Asp.* **2012**, *403*, 69–78. [CrossRef]

42. Miyamoto, N.; Kawai, R.; Kuroda, K.; Ogawa, M. Adsorption and aggregation of a cationic cyanine dye on layered clay minerals. *Appl. Clay Sci.* **2000**, *16*, 161–170. [CrossRef]

43. Lagaly, G.; Ogawa, M.; Dékány, I. Chapter 10.3—Clay Mineral-Organic Interactions. *Dev. Clay Sci.* **2013**, *5*, 215–225.

44. El Mouzdahir, Y.; Elmchaouri, A.; Mahboub, R.; Gil, A.; Korili, S.A. Equilibrium modeling for the adsorption of methylene blue from aqueous solutions on activated clay minerals. *Desalination* **2010**, *250*, 335–338. [CrossRef]

45. Yuan, G.; Theng, B.; Churchman, G.; Gates, W. Clays and Clay Minerals for Pollution Control. *Dev. Clay Sci.* **2013**, *5*, 587–644.

46. Vargas-Rodríguez, Y.M.; Obaya, A.; García-Petronilo, J.E.; Vargas-Rodríguez, G.I.; Gómez-Cortés, A.; Tavizón, G.; Chávez-Carvayar, J.A. Adsorption Studies of Aqueous Solutions of Methyl Green for Halloysite Nanotubes: Kinetics, Isotherms, and Thermodynamic Parameters. *Am. J. Nanomater.* **2021**, *9*, 1–11. [CrossRef]

47. Ali, I.; Asim, M.; Khan, T.A. Low cost adsorbents for the removal of organic pollutants from wastewater. *J. Environ. Manag.* **2012**, *113*, 170–183. [CrossRef] [PubMed]

48. Özcan, A.S.; Erdem, B.; Özcan, A. Adsorption of acid blue 193 from aqueous solutions onto Na-bentonite and DTMA-bentonite. *J. Colloid Interface Sci.* **2004**, *280*, 44–54. [CrossRef] [PubMed]

49. Liu, R.; Zhang, B.; Mei, D.; Zhang, H.; Li, J. Adsorption of methyl violet from aqueous solution by halloysite nanotubes. *Desalination* **2011**, *268*, 111–116. [CrossRef]

50. Chowdhury, S.; Mishra, R.; Saha, P.; Kushwaha, P. Adsorption thermodynamics, kinetics and isosteric heat of adsorption of malachite green onto chemically modified rice husk. *Desalination* **2011**, *265*, 159–168. [CrossRef]

51. Hasani, N.; Selimi, T.; Mele, A.; Thaçi, V.; Halili, J.; Berisha, A.; Sadiku, M. Theoretical, Equilibrium, Kinetics and Thermodynamic Investigations of Methylene Blue Adsorption onto Lignite Coal. *Molecules* **2022**, *27*, 1856. [CrossRef]

52. Berisha, A.; Podvorica, F.I.; Vataj, R. Corrosion Inhibition Study of Mild Steel in an Aqueous Hydrochloric Acid Solution Using Brilliant Cresyl Blue—A Combined Experimental and Monte Carlo Study. *Port. Electrochim. Acta* **2021**, *39*, 393–401. [CrossRef]

53. Babas, H.; Khachani, M.; Warad, I.; Ajebli, S.; Guessous, A.; Guenbour, A.; Safi, Z.; Berisha, A.; Bellaouchou, A.; Abdelkader, Z.; et al. Sofosbuvir adsorption onto activated carbon derived from argan shell residue: Optimization, kinetic, thermodynamic and theoretical approaches. *J. Mol. Liq.* **2022**, *356*, 119019. [CrossRef]

54. Sun, H.; Jin, Z.; Yang, C.; Akkermans, R.L.C.; Robertson, S.H.; Spenley, N.A.; Miller, S.; Todd, S.M. COMPASS II: Extended coverage for polymer and drug-like molecule databases. *J. Mol. Model.* **2016**, *22*, 47. [CrossRef]

55. Dagdag, O.; Berisha, A.; Safi, Z.; Dagdag, S.; Berrani, M.; Jodeh, S.; Verma, C.; Ebenso, E.E.E.E.; Wazzan, N.; El Harfi, A. Highly durable macromolecular epoxy resin as anticorrosive coating material for carbon steel in 3% NaCl: Computational supported experimental studies. *J. Appl. Polym. Sci.* **2020**, *137*, 49003. [CrossRef]

56. Berisha, A. The influence of the grafted aryl groups on the solvation properties of the graphyne and graphdiyne—A MD study. *Open Chem.* **2019**, *17*, 703–710. [CrossRef]

57. Crini, G.; Peindy, H.N.; Gimbert, F.; Robert, C. Removal of C. I. Basic Green 4 (Malachite Green) from Aqueous Solutions by Adsorption Using Cyclodextrin-based Adsorbent: Kinetic and Equilibrium Studies. *Sep. Purif. Technol.* **2007**, *53*, 97–110. [CrossRef]

58. Hussin, M.Z.; Talib, N.; Hussin, M.N.; Hanafiah, A.K.M.M.; Khalir, K.A.W.M.W. Methylene Blue Adsorption onto NaOH Modified Durian Leaf Powder: Isotherm and Kinetic Studies. *Am. J. Environ. Eng.* **2015**, *5*, 38–43.

59. Ahmad, R.; Kumar, R. Adsorption studies of hazardous malachite green onto treated ginger waste. *J. Environ. Manag.* **2010**, *91*, 1032–1038. [CrossRef]

60. Khattri, S.D.; Singh, M.K. Removal of malachite green from dye wastewater using neem sawdust by adsorption. *J. Hazard. Mater.* **2009**, *167*, 1089–1094. [CrossRef] [PubMed]

61. Mahini, R.; Esmaeili, H.; Foroutan, R. Adsorption of methyl violet from aqueous solution using brown algae Padina sanctae-crucis. *Turk. J. Biochem.* **2018**, *43*, 623–631. [CrossRef]

62. Mane, V.S.; Deo Mall, I.; Chandra Srivastava, V. Kinetic and equilibrium isotherm studies for the adsorptive removal of Brilliant Green dye from aqueous solution by rice husk ash. *J. Environ. Manag.* **2007**, *84*, 390–400. [CrossRef] [PubMed]

63. Ukkund, S.J.; Puthiyillam, P.; Anqi, A.E.; Taqui, S.N.; Ali, M.A.; Syed, U.T.; Alghamdi, M.N.; Siddiqui, M.I.H.; Alshehri, H.M.; Safaei, M.R.; et al. A Recent Study on Remediation of Direct Blue 15 Dye Using Halloysite Nanotubes. *Appl. Sci.* **2021**, *11*, 8196. [CrossRef]

64. Afroze, S.; Sen, T.K.; Ang, M.; Nishioka, H. Adsorption of methylene blue dye from aqueous solution by novel biomass *Eucalyptus sheathiana* bark: Equilibrium, kinetics, thermodynamics and mechanism. *Desalination Water Treat.* **2016**, *57*, 5858–5878. [CrossRef]

65. Ghodbane, I.; Hamdaoui, O. Removal of mercury (II) from aqueous media using eucalyptus bark: Kinetic and equilibrium studies. *J. Hazard. Mater.* **2008**, *160*, 301–309. [CrossRef] [PubMed]

66. Ponnusami, V.; Vikram, S.; Srivastava, S. Guava (*Psidium guajava*) leaf powder: Novel adsorbent for removal of methylene blue from aqueous solutions. *J. Hazard. Mater.* **2008**, *152*, 276–286. [CrossRef] [PubMed]

67. Ponnusami, V.; Gunasekar, V.; Srivastava, S. Kinetics of methylene blue removal from aqueous solution using gulmohar (*Delonix regia*) plant leaf powder: Multivariate regression analysis. *J. Hazard. Mater.* **2009**, *169*, 119–127. [CrossRef] [PubMed]

68. Kumar, P.S.; Ramalingam, S.; Sathishkumar, K. Removal of methylene blue dye from aqueous solution by activated carbon prepared from cashew nut shell as a new low-cost adsorbent. *Korean J. Chem. Eng.* **2011**, *28*, 149–155. [CrossRef]

69. Zhao, M.; Liu, P. Adsorption behavior of methylene blue on halloysite nanotubes. *Microporous Mesoporous Mater.* **2008**, *112*, 419–424. [CrossRef]

70. Dahri, M.K.; Kooh, M.R.R.; Lim, L.B.L. Removal of Methyl Violet 2B from Aqueous Solution Using *Casuarina equisetifolia* Needle. *ISRN Environ. Chem.* **2013**, *8*. [CrossRef]

71. Yener, J.; Kopac, T.; Dogu, G.; Dogu, T. Adsorption of Basic Yellow 28 from aqueous solutions with clinoptilolite and amberlite. *J. Colloid Interface Sci.* **2006**, *294*, 255–264. [CrossRef] [PubMed]

72. Fil, B.A.; Yilmaz, M.T.; Bayar, S.; Elkoca, M.T. Investigation of adsorption of the dyestuff astrazon red violet 3rn (basic violet 16) on montmorillonite clay. *Braz. J. Chem. Eng.* **2014**, *31*, 171–182. [CrossRef]

73. Langmuir, I. The adsorption of gases on plane surfaces of glass, mica and platinum. *J. Am. Chem.* **1918**, *40*, 1361–1403. [CrossRef]

74. Irannajad, M.; Haghighi, K.H.; Safarzade, E. Kinetic, thermodynamic and equilibrium studies on the removal of copper ions from aqueous solutions by natural and modified clinoptilolites. *Korean J. Chem. Eng.* **2015**, *32*, 1–11. [CrossRef]

75. Khan, T.; Dahiya, A.S.; Ali, I. Use of kaolinite as adsorbent: Equilibrium, dynamics and thermodynamic studies on the adsorption of Rhodamine B from aqueous solution. *Appl. Clay Sci.* **2012**, *69*, 58–66. [CrossRef]

76. Hu, Q.; Zhang, Z. Application of Dubinin–Radushkevich isotherm model at the solid/solution interface: A theoretical analysis. *J. Mol. Liq.* **2018**, *277*, 646–648. [CrossRef]

77. Mittal, H.; Kumar, V.; Saruchi; Ray, S.S. Adsorption of methyl violet from aqueous solution using gum xanthan/Fe$_3$O$_4$ based nanocomposite hydrogel. *Int. J. Biol. Macromol.* **2016**, *89*, 1–11. [CrossRef]

78. Bertolini, T.C.; Izidoro, J.D.; Magdalena, C.P.; Fungaro, D.A. Adsorption of Crystal Violet Dye from Aqueous Solution onto Zeolites from Coal Fly and Bottom Ashes. *Orbital Electron. J. Chem.* **2013**, *5*, 179–191.

79. Hubbe, M.A.; Azizian, S.; Douven, S. Implications of apparent pseudo-second-order adsorption kinetics onto cellulosic materials: A review. *BioResources* **2019**, *43*, 7582–7626. [CrossRef]

80. Oloo, M.C.; Onyari, M.J.; Wanyonyi, C.W.; Wabomba, N.J.; Muinde, M.V. Adsorptive removal of hazardous crystal violet dye form aqueous solution using *Rhizophora mucronata* stem-barks: Equilibrium and kinetics studies. *Environ. Chem. Ecotoxicol.* **2020**, *2*, 64–72. [CrossRef]

81. Shee, A.; Onyari, J.M.; Wabomba, J.N.; Munga, D. Methylene Blue Adsorption onto Coconut husks/Polylactide Blended Films: Equilibrium and Kinetic Studies. *Chem. Mater. Res.* **2014**, *6*, 28–37.

82. Cheruiyot, G.K.; Wanyonyi, W.C.; Kiplimo, J.J.; Maina, E.N. Adsorption of toxic crystal violet dye using coffee husks: Equilibrium, kinetics and thermodynamics study. *Sci. Afr.* **2019**, *5*, e00116. [CrossRef]

83. Tran, H.N.; You, S.J.; Chao, H.P. Thermodynamic parameters of cadmium adsorption onto orange peel calculated from various methods: A comparison study. *J. Environ. Chem. Eng.* **2016**, *4*, 2671–2682. [CrossRef]

84. Xie, S.; Zhang, C.; Zhou, X.; Yang, J.; Zhang, X.; Wang, J. Comments on "removal of uranium (VI) from aqueous solution by adsorption of hematite". *J. Environ. Radioact.* **2009**, *100*, 921–922.

85. Chiou, M.S.; Li, H.Y. Adsorption behaviour of reactive dye in aqueous solution on chemical cross-linked chitosan beads. *Chemosphere* **2003**, *50*, 1095–1105. [CrossRef]

86. Nollet, H.; Roels, M.; Lutgen, P.; Van der Meeren, P.; Verstraete, W. Removal of PCBs from wastewater using fly ash. *Chemosphere* **2003**, *53*, 655–665. [CrossRef]